Cross-streamer wavefield interpolation using deep convolutional neural network

Thomas Larsen Greiner[1,2] , Odd Kolbjørnsen[1,2], Jan Erik Lie[1], Espen Harris Nilsen[1], Andreas Kjelsrud Evensen[1] and Leiv Gelius[2]. [1]Lundin Norway , [2]University of Oslo

Summary

Seismic exploration in complex geological settings and shallow geological targets has led to a demand for higher spatial and temporal resolution in the final migrated image. Seismic data from conventional marine acquisition lacks near offset and wide azimuth data, which limits imaging in these settings. In addition, large streamer separation introduce aliasing of spatial frequencies across the streamers. A new marine survey configuration, known as TopSeis, was introduced in 2017 in order to address the shallow-target problem. However, introduction of near offset data has shown to be challenging for interpolation and regularization, using conventional methods. In this paper, we investigate deep learning as a tool for interpolation beyond spatial aliasing across the streamers, in the shot domain. The proposed method is based on imaging techniques from single-image super resolution (SISR). The model architecture consist of a deep convolutional neural network (CNN) and a periodic resampling layer for upscaling to the non-aliased wavefield. We demonstrate the performance of proposed method on representative broad-band synthetic data and TopSeis field data from the Barents Sea.

Introduction

In conventional 3D marine seismic surveys, the seismic wavefield is recorded by sensors placed uniformly on a spread of ten or more streamers that are towed by a single vessel utilizing two airgun source arrays in front of the streamers. The shot domain receiver seperation in the inline direction is typically in the interval of 12.5 m, and 100 m to 75 m in the crossline direction. Data acquired in this way lack near offset and wide azimuth data. Thus limiting the amount of recorded reflected energy, especially in situations with large velocity contrasts in the shallow. Seismic imaging benefits from near offset data in order to record the narrow cone of reflected energy in these velocity-depth settings (Lie et al., 2018). In order to address the shallow-target seismic-imaging issue, CGG and Lundin Norway proposed in 2017 a tailored acquisition solution, known as TopSeis (Vinje et al., 2017), yielding improved recording of the the near offsets. This acquisition solution utilize a split-spread, source-over-cable configuration, reduced streamer separation (50 m), wider source separation and deploying more than two sources. However, near offset data are sparse and suffers from spatial aliasing, and necessary processing steps like interpolation and data-regularization have shown to be challenging using conventional methods.

Several seismic interpolation methods exists. Some methods assumes local linearity, interpolating in the frequency-space domain using error prediction filters (Spitz, 1991; Crawley, 2001; Naghizadeh and Sacchi, 2009; Naghizadeh and Sacchi, 2012). Other interpolation methods reconstruct the wavefield by means of sparse signal transform, such as Fourier (Zwartjes and Sacchi, 2007; Schonewille et al., 2009; Naghizadeh and Sacchi, 2010a; Gao et al., 2013), Radon (Ibrahim et al., 2015), Curvelet (Naghizadeh and Sacchi, 2010b), Seislet (Gan et al., 2015) and Focal (Kutscha et al., 2010). In addition, utilizing information from multicomponent data in combination with sparse optimization, the crossline reconstruction beyond aliasing is possible (Robertson et al., 2008; Özbek et al., 2010; Özdemir et al., 2010; Vassallo et al., 2010). More recent studies using learning-based approaches such as dictionary learning (Turquais et al. 2018), support vector regression (Jia and Ma, 2017) and CNN (Wang et al., 2019).

We investigate deep learning as a data driven approach for interpolation beyond aliasing, across the streamers in the shot domain. Our approach to the seismic interpolation problem could be seen as an analogy to inverse problems in image scaling for resizing low-resolution (LR) digital images to their corresponding high-resolution (HR) counterpart. These set of techniques are usually referred to as super resolution (SR) imaging (Yang et al., 2018). We start by training an interpolation function on streamers in the inline direction that are downscaled to imitate the crossline streamer seperation. With the assumption that the inline wavefield is representative for the crossline wavefield, we apply the trained function in the crossline direction. In our approach, the input to the CNN model is in LR-space, and a reconstructed counterpart in HR-space, through upscaling only in the output layer. The upscaling is done through a periodic resampling method similar to the SubPixel convolution layer in Shi et al. (2016). The synthetic data examples in addition to the TopSeis field data examples demonstrate the performance of our proposed method.

Theory

Consider training data $\mathfrak{D} = \{\boldsymbol{Y}_i^{\mathrm{HR}}, \boldsymbol{Y}_i^{\mathrm{LR}}\}_{i=1}^{M}$, where $\boldsymbol{Y}_i^{\mathrm{HR}}$ is defined by a shot-cable pair in the inline direction in HR-space and $\boldsymbol{Y}_i^{\mathrm{LR}}$ is the corresponding downsampled counterpart in LR-space. Our objective is then to design and train a function $f : \boldsymbol{Y}^{\mathrm{LR}} \rightarrow \boldsymbol{Y}^{\mathrm{HR}}$, which preserves the characteristics of the non-aliased wavefield. Let N_l denote the number of features and $k_l = 1,2, \dots, N_l$ denote the k'th

10.1190/segam2019-3214009.1

convolutional filter in layer l. The k'th non-linear output from an arbitrary layer to the next can be defined as

$$\boldsymbol{a}_{k_l}^{[l]} = \varphi^{[l]}\left(\boldsymbol{W}_{k_l}^{[l]} * \boldsymbol{a}^{[l-1]} + \boldsymbol{b}_{k_l}^{[l]}\right) \quad (1)$$

where $\boldsymbol{W}_{k_l}^{[l]} \in \mathbb{R}^{f_l \times f_l \times N_{l-1}}$ is the weights and $\boldsymbol{b}_{k_l}^{[l]} \in \mathbb{R}$ are the biases, which defines the learnable parameters. In (1), $\boldsymbol{a}^{[l-1]}$ defines all non-linear outputs from layer $l-1$. The function $\varphi^{[l]}$ provides non-linearity between the layers and is given in our case by the Leaky Rectified Linear Unit (Maas et al., 2013). The output layer is given by what we will refer to as the spatial periodic resampling (SPR) layer

$$\widehat{\boldsymbol{Y}}^{\mathrm{HR}} = SPR\left(\boldsymbol{W}_{k_l}^{[L]} * \boldsymbol{a}^{[L-1]} + \boldsymbol{b}_{k_l}^{[L]}, \boldsymbol{a}^{[0]}\right) \quad (2)$$

where $SPR(\cdot)$ is a periodic resampling process between the input and the feature maps in the last convolution layer.The proposed CNN has $L = 5$ hidden layers. A conceptual sketch is shown in Figure 1. The model is fittet using an objective function given by the L_1norm between the output and the target including L_2 regularization on the weights

$$\mathcal{L}(\boldsymbol{W}, \boldsymbol{b}) = \left\|\boldsymbol{Y}^{\mathrm{HR}} - \widehat{\boldsymbol{Y}}^{\mathrm{HR}}\right\|_1^1 + \frac{\boldsymbol{\lambda}}{2}\|\boldsymbol{W}\|_2^2 \quad (3)$$

where λ is the regularization parameter. For any $\boldsymbol{\lambda} > 0$ the regularization term contributes to the objective function, constraining the weight values and therefore reducing the risk of overfitting. The optimization problem, i.e. finding $\boldsymbol{W}$ and $\boldsymbol{b}$ which minimize $\mathcal{L}(\boldsymbol{W}, \boldsymbol{b})$ was performed by a first-order gradient optimization algorithm known as ADAM optimizer (Kingma and Ba, 2015). Our model is implemented in python using the Tensorflow package (Abadi et al., 2015).

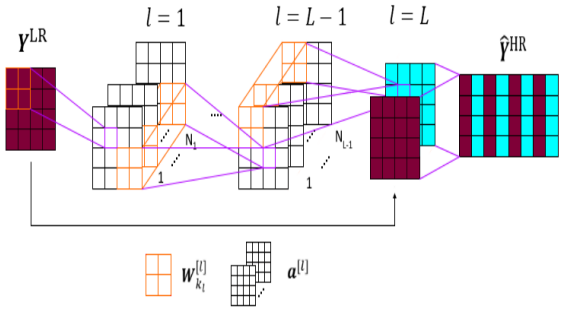

Figure 1: Conceptual sketch of the CNN architecture with the periodic resampling layer in the last layer with downscaling ratio of $r = 2$. Adapted from Shi et al. (2016).

Synthetic data examples

In this section, we demonstrate the performance of the proposed method by applying it on representative synthetic data. The data consist of diffraction modelled Broadband (2-190 Hz) data, with field recorded noise (Vinje et al., 2017). The receiver interval in the inline direction is $\Delta x = 12.5$ m, and crossline streamer separation is $\Delta y = 50$ m. Considering M training examples, the training data consist of the HR examples and their corresponding downscaled LR example $\mathfrak{D} = \{\boldsymbol{Y}_i^{\mathrm{HR}}, \boldsymbol{Y}_i^{\mathrm{LR}}\}_{i=1}^{M}$. The dimension of the training examples was 201×80 for $\boldsymbol{Y}^{\mathrm{HR}}$ and 201×20 for $\boldsymbol{Y}^{\mathrm{LR}}$. The first and second dimension denote the number of time samples and number of receivers respectively. The second dimension implies a downscaling ratio of $r = 4$. The training data consists of 500 shots, with each shot having a spread of 14 cables, yielding $M = 7000$ training examples. The training data is split into a training set, a validation set and a test set with a distribution of $60/20/20$. The reason why we split them into three separate sets, is to have two datasets (training and validation) for training and tuning the model, and one dataset (test set) as unseen data, yielding an unbiased estimation for the final score. Furthermore, training deep models benefits from large training sets in terms of test loss and generalization error (Zhang et al, 2017). Therefore, we increase the training set size by data augmentation, which yielded a total of 33600 examples for the training set.

When the model is fully trained we predict the HR data in the test set by running the model on the corresponding LR test data. The interpolation result from an arbitrary example in the test set (in the inline direction) is presented in time-space domain in Figure 2 and in the frequency-wavenumber in Figure 3. As shown in Figure 2 and Figure 3, the results are encouraging when comparing to the target data. Visually, the target- and interpolated wavefield are close to equal. Even in the case of 75% missing traces, the trained model demonstrates that it is able to reconstruct and preserve the characteristics of the non-aliased wavefield, and able to handle linear, curved and interfering events. For a quantitative measurement we measured the recovered peak signal to noise ratio (PSNR), which gave for the test set example 32.60. The average PSNR for the data sets are 32.98 (training), 33.05 (validation) and 32.99 (test), indicating reasonable recovery for the unseen test set. Since the main objective is to interpolate the missing traces in the crossline direction, we sort the test set to crossline direction, and apply the trained model. The results are shown in Figure 4 in the time-space domain, and the frequency-wavenumber domain in Figure 5. From the frequency-wavenumber domain, in Figure 3 and 5, we observe that interpolated result are similar to what we observe in the inline case.

10.1190/segam2019-3214009.1

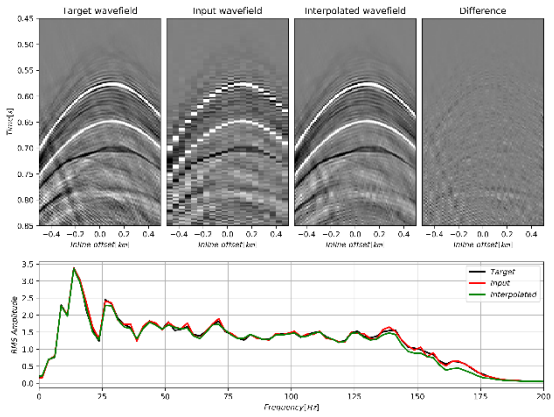

Figure 2: Synthetic data reconstruction result from a shot-cable pair, from the test set in the inline direction. The target was downscaled by a ratio of $r = 4$.

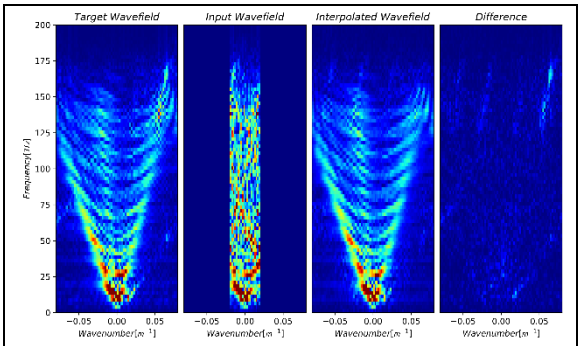

Figure 3: Reconstruction result from a shot-cable pair from Figure 2 in the frequency-wavenumber domain.

Field data examples

In this section, we demonstrate the performance of the proposed method by applying it on TopSeis data from the Barents Sea. The training data consist of 1000 shots, with each shot having a spread of 14 cables. The setup in the field data example is equal to the synthetic example. The training data is split into a training set, a validation set and a test set with a distribution of 72/8/20 respectively. The training data is augmented, which yielded 80800 examples for the training set. We predict the HR data in the test set by applying the model (trained on field data) on the corresponding LR test data. The field data result from an arbitrary example in the test set, (in the inline direction), is presented in time-space domain in Figure 6 and in the frequency-wavenumber domain in Figure 7. Similar to the synthetic examples, the model demonstrates good performance in terms of PSNR recovery and reconstructs a promising non-aliased wavefield.

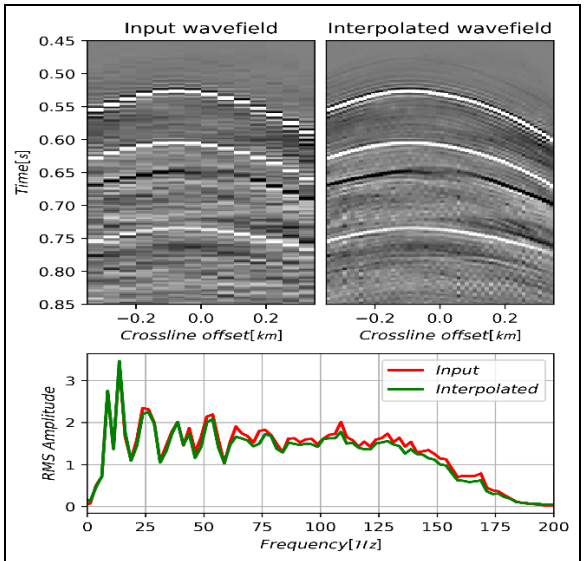

Figure 4: Synthetic data reconstruction result from the test set in the crossline direction.

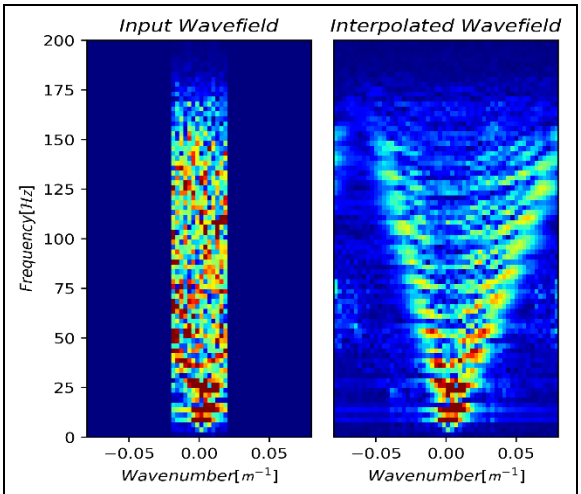

Figure 5: Synthetic data reconstruction result in the frequency-wavenumber domain, from the test set shown in Figure 4.

The PSNR for the test set example is 26.39. The average PSNR for the data sets are 27.33 (training), 27.46 (validation) and 27.37 (test), indicating reasonable recovery for the unseen test set. However, in these examples the model struggles more with frequencies above 30 Hz compared to the synthetic example. Visually, the prediction contains less noise than the target, and it is likely that the some of observed difference in energy corresponds to the noise, which the model has not been able to interpolate. We

10.1190/segam2019-3214009.1

also observe continuous events in the residual, which is not reconstructed by the model.

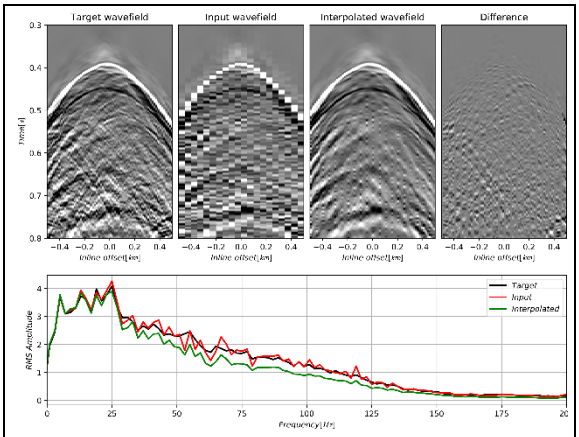

Figure 6: Field data reconstruction result from a shot-cable pair, from the test set in the inline direction. The target was downscaled by a ratio of $r = 4$.

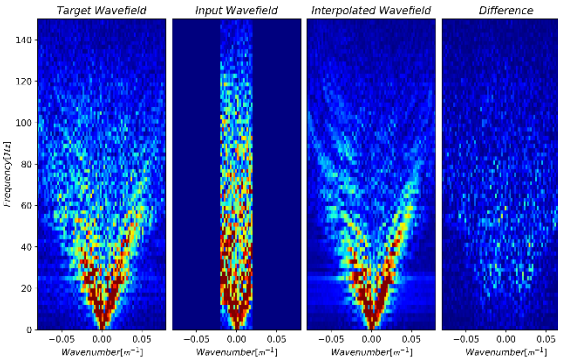

Figure 7: Field data reconstruction result from the shot-cable shown in Figure 6, in the frequency-wavenumber domain.

Conclusions

In this abstract, we propose a data driven approach for seismic interpolation across the streamer. We train a deep CNN model to learn the characterics of the wavefield in the inline direction, and apply the model to the crossline direction. We show that the trained models are able to interpolate beyond aliasing across the streamers, and preserve the characteristics of the non-aliased wavefield. In the synthetic example we were able to interpolate Broadband data with recorded field noise added, with minor residuals. However, the field data example show that the model struggles more with frequencies above 30 Hz, than in the synthetic example. It is likely that the non-interpolated energy could both correspond to noise and/or events which is not contained within the input. More work is necessary in order to address the high frequency issues.

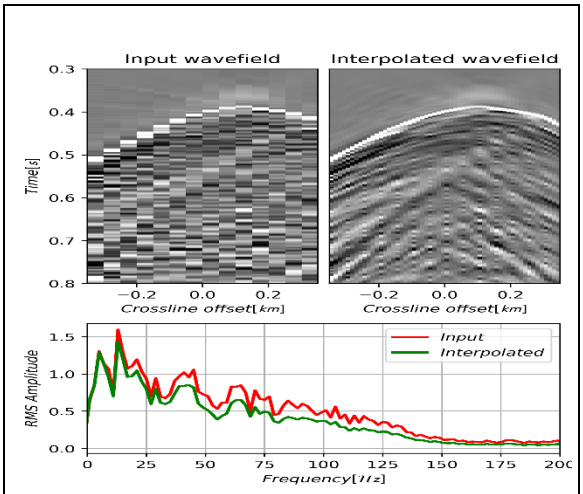

Figure 8: Field data reconstruction result from the test set in the crossline direction.

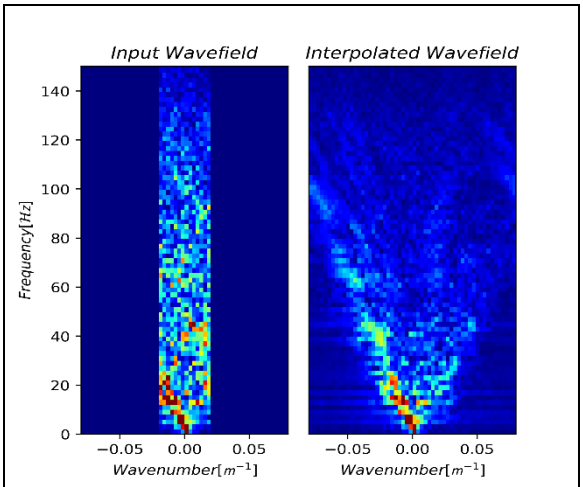

Figure 9: Field data reconstruction result in the frequency-wavenumber domain, from the test set shown in Figure 8.

Acknowledgements

This research is financially supported by the Research Council of Norway, project number 287664. We thank Lundin-Norway for permission to publish this work.

10.1190/segam2019-3214009.1

REFERENCES

Abadi, M., A. Agarwal, P. Barham, E. Brevdo, Z. Chen, C. Citro, G. S. Corrado, A. Davis, J. Dean, M. Devin, S. Ghemawat, I. Goodfellow, A. Harp, G. Irving, M. Isard, R. Jozefowicz, Y. Jia, L. Kaiser, M. Kudlur, J. Levenberg, D. Mané, M. Schuster, R. Monga, S. Moore, D. Murray, C. Olah, J. Shlens, B. Steiner, I. Sutskever, K. Talwar, P. Tucker, V. Vanhoucke, V. Vasudevan, F. Viégas, O. Vinyals, P. Warden, M. Wattenberg, M. Wicke, Y. Yu, and X. Zheng, 2015, TensorFlow: Large-scale machine learning on heterogeneous systems: Software available from https://doi.org/tensorflow.org.

Crawley, S., 2001, Seismic trace interpolation with nonstationary prediction-error filters: Ph.D. thesis, Stanford University.

Ibrahim, A., M. D. Sacchi, and P. Terenghi, 2015, Wavefield reconstruction using a stolt-based asymptote and apex shifted hyperbolic radon transform: 85th Annual International Meeting, SEG, Expanded Abstracts, 3836–3841, doi: https://doi.org/10.1190/segam2015-5873567.1.

Jia, Y., and J. Ma, 2017, What can machine learning do for seismic data processing? An interpolation application: Geophysics, **82**, no. 3, V163–V177, doi: https://doi.org/10.1190/GEO2016-0300.1.

Kingma, D. P., and J. Ba, 2015, Adam: A method for stochastic optimization: ICLR.

Kutscha, H., D. E. Verschuur, and A. G. Berkhout, 2010, High resolution double focal transformation and its application to data reconstruction: 80th Annual International Meeting, SEG, Expanded Abstracts, 3589–3593, doi: https://doi.org/10.1190/1.3513595.

Lie, J. E., Danielsen, V., Dhelie, P. E., Sablon, R., Siliqi, R., Grubb, C., Vinje, V., Nilsen, C. I., and Soubaras, R., 2018, A novel source-over-cable solution to address the Barents Sea imaging challenges: Marine Acquisition Workshop.

Maas, A. L., A. Y. Hannun, and A. Y. Ng, 2013, Rectifier nonlinearities improve neural network acoustic models: In ICML.

Naghizadeh, M., 2012, Seismic data interpolation and denoising in the frequency-wavenumber domain: Geophysics, **77**, no. 2, V71–V80, doi: https://doi.org/10.1190/geo2011-0172.1.

Naghizadeh, M., and M. Sacchi, 2009, f-x adaptive seismic-trace interpolation: Geophysics, **74**, no. 1, V9–V16, doi: https://doi.org/10.1190/1.3008547.

Naghizadeh, M., and M. Sacchi, 2010b, Hierarchical scale curvelet interpolation of aliased seismic data: 80th Annual International Meeting, SEG, Expanded Abstracts, 3656–3661, doi: https://doi.org/10.1190/1.3513610.

Naghizadeh, M., and M. D. Sacchi, 2010a, On sampling functions and Fourier reconstruction methods: Geophysics, **75**, no. 6, WB137–WB151, doi: https://doi.org/10.1190/1.3503577.

Özbek, A., M. Vassallo, K. Ozdemir, D.-J. van Manen, and K. Eggenberger, 2010, Crossline wavefield reconstruction from multicomponent streamer data: Part 2. Joint interpolation and 3D up/down separation by generalized matching pursuit: Geophysics, **75**, no. 6, WB69–WB85, doi: https://doi.org/10.1190/1.3497316.

Özdemir, K., A. Özbek, D.-J. van Manen, and M. Vassallo, 2010, On dataindependent multicomponent interpolators and the use of priors for optimal reconstruction and 3D up/down separation of pressure wavefields: Geophysics, **75**, no. 6, WB39–WB51, doi: https://doi.org/10.1190/1.3494621.

Robertsson, J. O., I. Moore, M. Vassallo, K. Özdemir, D.-J. van Manen, and A. Özbek, 2008, On the use of multicomponent streamer recordings for reconstruction of pressure wavefields in the crossline direction: Geophysics, **73**, no. 5, A45–A49, doi: https://doi.org/10.1190/1.2953338.

Schonewille, M., A. Klaedtke, and A. Vigner, 2009, Antialias antileakage Fourier transform: 79th Annual International Meeting, SEG, Expanded Abstracts, 3249–3253, doi: https://doi.org/10.1190/1.3255533.

Shi, W., J. Caballero, F. Huszár, J. Totz, A. P. Aitken, R. Bishop, D. Rueckert, and Z. Wang, 2016, Real-time single image and video super-resolution using an efficient sub-pixel convolutional neural network: IEEE Conference on Computer Vision and Pattern Recognition, 1874–1883.

Spitz, S., 1991, Seismic trace interpolation in the F-X domain: Geophysics, **56**, 785–794, doi: https://doi.org/10.1190/1.1443096.

Turquais, P., E. G. Asgedom, W. Sölner, and L. Gelius, 2018, Parabolic dictionary learning for seismic wavefield reconstruction across the streamers: Geophysics, **83**, no. 4, V263–V282, doi: https://doi.org/10.1190/geo2017-0694.1.

Vassallo, M., A. Ozbek, K. Ozdemir, and K. Eggenberger, 2010, Crossline wavefield reconstruction from multicomponent streamer data. Part 1: Multichannel interpolation by matching pursuit (MIMAP) using pressure and its crossline gradient: Geophysics, **75**, no. 6, WB53–WB67, doi: https://doi.org/10.1190/1.3496958.

Vinje, V., J. E. Lie, V. Danielsen, P. E. Dhelie, R. Siliqi, C. I. Nilsen, E. Hicks, and A. Camerer, 2017, Shooting over the seismic spread: First Break, **35**.

Wang, B., N. Zhang, W. Lu, and J. Wang, 2019, Deep-learning-based seismic data interpolation: A preliminary result: Geophysics, **84**, no. 1, V11–V20, doi: https://doi.org/10.1190/geo2017-0495.1.

Yang, W., X. Zhang, Y. Tian, W. Wang, and J. H. Xue, 2018, Deep learning for single image super-resolution: a brief review: arXiv preprint arXiv:1808.03344.

Zhang, C., S. Bengio, M. Hardt, B. Recht, and O. Vinyals, 2017, Understanding deep learning requires rethinking generalization: ICLR.

Zwartjes, P. M., and M. D. Sacchi, 2007, Fourier reconstruction of nonuniformly sampled, aliased seismic data: Geophysics, **72**, no. 1, V21–V32, doi: https://doi.org/10.1190/1.2399442.